Chaos
An Interdisciplinary Journal
of Nonlinear Science

AIP Publishing

Network structure and time delays shape synchronisation patterns in brain network models

Iain Pinder,[1] Martin R. Nelson,[1] and Jonathan J. Crofts[1]
School of Science and Technology, Department of Physics and Mathematics, Nottingham Trent University, Nottingham, NG11 8NS, UK

(*Electronic mail: jonathan.crofts@ntu.ac.uk)

(Dated: 7 October 2024)

In this paper we investigate synchronisation patterns and coherence for a network of delayed Wilson-Cowan nodes. To capture information processing across different brain regions, our model incorporates two distinct delays: an intra-nodal delay that reflects the time signals take to travel within a cortical region due to local circuitry; and an inter-nodal delay representing the longer communication times associated with white matter connections between brain areas. To investigate the role of network topology we consider a range of toy network structures as well as the known (macro-scale) cortical structure of the Macaque monkey. We examine how global network dynamics are shaped by a combination of network configuration, coupling strength and time delays. Our focus lies on two dynamic measures: synchrony and metastability, the latter reflecting the temporal variation of the former, both crucial for the brain's real-time functionality. Our investigation identifies extensive regions within the system's parameter space where the synchronised state exhibits transverse instabilities. These instabilities give rise to diverse dynamical behaviors contingent upon the network architecture and the interplay between coupling strength and time delay. While similar complex partially synchronised states existed for all network topologies considered, the cortical network demonstrated time-dependent behaviors, such as phase cluster dynamics, which were absent in the toy network architectures, and which are considered crucial in its ability to orchestrate complex information processing and behaviour. Additionally, we illustrate how delays can regulate a cortical network with chaotic local dynamics, thus emphasising the potential importance of delays in suppressing pathological spreading dynamics.

Investigating synchronization in large-scale neural networks is a cornerstone of understanding cognitive function. Neural ensembles exhibit a broad spectrum of oscillatory activity, and their transient coupling (synchronisation) is believed to be a fundamental mechanism underlying perception, attention, and motor control. This synchronisation is not simply a global phenomenon, but rather a complex interplay between local and long-distance connections within the brain. Employing a modeling approach, this study investigates the dynamical properties of large-scale brain networks. We focus on synchrony and its variability, a measure considered a proxy for metastability. These properties are thought to be critical for the brain's real-time functional coordination during cognition and behavior. For all considered network structures, we find regions of existence for synchrony, partial synchrony, and irregular, chaotic-like dynamics. Notably, only the cortical network exhibited emergent phase cluster dynamics, which were contingent upon specific dynamical parameters. This suggests that such flexible synchronisation patterns might be a hallmark of functional interactions within the brain, allowing for transitions between network configurations.

I. INTRODUCTION

Network neuroscience offers a comprehensive framework with which to investigate large-scale networks emerging from contemporary neuroimaging techniques describing both structural and functional connectivities within the brain[1–3]. Observed oscillatory patterns of neural activity spanning multiple spatial scales naturally arise throughout the brain, and are believed to be a consequence of its underlying topological features such as the strength and location of synapses as well as the presence of feedback loops[4]. Investigating the mechanisms that govern the synchronisation and propagation of neural activity is a fundamental objective of network neuroscience[5–8].

A recent approach that promises to improve our comprehension of the intricate relations between structure and function in the brain involves the utilisation of brain network models (BNMs)[9]. These models integrate detailed anatomical connectivity data with simulated neural activity, enabling the replication of large-scale brain functional connectivity such as that observed using modern imaging tools. Population models are widely used to simulate large-scale brain activity[10–12] since they offer a computationally efficient yet biologically plausible approach to generating physiologically realistic brain states. A notable benefit of such an approach is that it enables researchers to conduct virtual experiments that serve predictive purposes and facilitate the testing of various experimental and clinical scenarios[13]. Thus research in this area potentially paves the way for personalised treatments in the field of neuroscience[14,15].

One important aspect of any BNM is that it accurately accounts for the effects of finite conduction velocities within the brain on observed spatiotemporal patterns of neural activity[16]. For large-scale BNMs, such as those considered in this work, there are two main sources of delay: inter-nodal delays that arise between distant populations of excitatory neurons; and intra-nodal delays that describe delayed self- or cross-interactions between localised populations of excitatory and

inhibitory neurons. However, most BNM studies focus on inter-nodal delays only. They are either empirical studies that incorporate long-distance pathway delays to replicate observed neural dynamics[17–19], or theoretical studies that use simplifying assumptions (such as a constant delay) to understand basic brain network properties, such as stability and synchronisation[20,21].

Recently, Conti and Van Gorder[22] considered the effects of inter- and intra-nodal delays on a system of coupled masses[2] via a numerical simulation. Deploying a range of model topologies, such as a path network, a ring network and a lattice network, they found that when coupled with neural delays, network structure had the ability to both regularise and deregularise network dynamics, depending upon the network's heterogeneity. One of the main goals of the current work is to further explore some of these ideas by simulating neural dynamics on a range of topologies, including both artificial and experimental architectures, thereby extending the work of Conti and Van Gorder to a more physiologically relevant setting.

In this paper we consider a BNM consisting of a network of coupled masses, or brain regions, the activity of which will be described by interacting populations of excitatory and inhibitory neurons, in accord with the standard Wilson-Cowan model[23]. The model incorporates both intra- and inter-nodal delays and we consider both model connectivity structures, such as a path, ring, lattice and complete network, as well as the known cortical network of the Macaque monkey[24,25]. Deploying numerical simulations we investigate the effect of inter-nodal delays and coupling strength on the network dynamics and complex spatiotemporal patterns for the aforementioned topologies. Moreover, given the growing evidence that brain network dynamics operate in a metastable regime, that maximises neural flexibility[26], this study aims to identify parameter values within our model that promote this optimal state of dynamic balance. We also analyse the extent to which cortical topology and delays can be used to regularise aperiodic pathological neural activity, an important aspect for the understanding of seizure disorders.

The structure of the paper is as follows. In §II we begin by providing some of the necessary prerequisites in network science, before moving on to describe the neural activity model deployed in our BNM in detail. We conclude the section by providing a brief overview of the different network architectures considered in our work, which includes a number of toy network structures as well as the cortical network of the Macaque monkey. In §III we investigate the role that coupling strength and inter-nodal delays play in the emergence of synchronous brain activity, as well as considering the extent to which cortical architecture can regularise pathological aperiodic brain activity. We conclude in §IV with a brief summary of our results and suggest a number of directions for future study.

II. METHODS

A. Network basics

Here, we consider simple networks (undirected, unweighted) that are defined in terms of an adjacency matrix $A \in \mathbb{R}^{n\times n}$, which has $a_{ij} = a_{ji} = 1$ if nodes i and j are connected, and $a_{ij} = a_{ji} = 0$ otherwise. We also have $a_{ii} = 0$ since self-links are disallowed.

Given an adjacency matrix many network statistics can be readily computed. For example, the degree of node i is given by $k_i = \sum_j a_{ij}$, and the mean degree is given by

$$\langle k\rangle = \frac{1}{n}\sum_{i=1}^{n} k_i = \frac{2m}{n},$$

where here m is the number of edges in the network. Degree heterogeneity, which is known to heavily impact the ability for nodes to synchronise their dynamics[27,28], can be quantified using Estrada's heterogeneity index[29]:

$$\sigma = \frac{1}{n-2\sqrt{n-1}} \sum_{(i,j)\in E} \left(\frac{1}{\sqrt{k_i}} - \frac{1}{\sqrt{k_j}}\right)^2.$$

Here, the sum is over all network edges, *i.e.* the collection E of unordered pairs (i, j) such that $a_{ij} = 1$.

The global clustering coefficient is given by

$$C = \frac{1}{n}\sum_{i=1}^{n} C_i,$$

where C_i denotes the probability that two neighbours are connected. The characteristic path-length $\langle l\rangle$ is defined as the number of edges in the shortest path between two vertices, averaged over all node pairs. Note that many real-world networks, including cortical networks, have been observed to exhibit both a high clustering coefficient and a short average path length. These networks, collectively known as *small-world networks*[30], are believed to offer functional advantages such as enhanced information processing, coordination, and robustness (see the paper by Bassett and Bullmore[31] for a recent discussion specific to brain networks).

For further details on the aforementioned network measures see the text by Newman[32].

B. The model

In this work we deploy the brain network metapopulation model introduced by Conti and Van Gorder[22], which is an extension of the population model of Wilson and Cowan[23] to networks. The model considers two populations of excitatory and inhibitory neurons with neural activity being described by

the following system

$$\begin{aligned}\frac{\mathrm{d}u_i}{\mathrm{d}t} &= -u_i(t) + f(c_1 u_i(t-\tau) + c_2 v_i(t-\tau) + P \\ &\quad + \varepsilon \sum_j w_{ij} u_j(t-\rho)), \\ \frac{\mathrm{d}v_i}{\mathrm{d}t} &= -v_i(t) + f(c_3 u_i(t-\tau) + c_4 v_i(t-\tau) + Q),\end{aligned} \tag{1}$$

for $i = 1, 2, \ldots, n$. Here, u_i and v_i represent the synaptic activity of the excitatory and inhibitory populations, respectively, f denotes a firing rate function given by

$$f(x) = \frac{1}{1+e^{-\beta x}}, \tag{2}$$

and ε is the coupling strength. The parameters c_1, c_2, c_3 and c_4 denote the strengths of interactions between sub-populations within a node, whilst P and Q are control parameters representing basal inputs to each node. Additionally, the model includes an intra-nodal delay τ for information processing within brain regions and an inter-nodal delay ρ for signal transmission between them. Unless otherwise stated, in our experiments we chose $\beta = 60, P = 0.65, Q = 0.5, c_1 = c_3 = -1, c_2 = -0.4$, $c_4 = 0$ and $\tau = 0.5$, which results in a set of identical self-sustained oscillators when the coupling strength, ε, is set to zero[33].

The matrix $W \in \mathrm{R}^{n\times n}$ is the scaled adjacency matrix given by

$$W = D^{-1}A, \tag{3}$$

where D is the diagonal matrix of degrees, *i.e.*

$$D = \begin{pmatrix} k_1 & & \\ & \ddots & \\ & & k_n \end{pmatrix}. \tag{4}$$

It follows that the row-sum of the weight matrix W is constant:

$$\sum_{j=1}^{n} w_{ij} = 1; \tag{5}$$

a condition which ensures the existence of a fully synchronised solution to (1). For a detailed description of the conditions under which synchronous solutions exist, see Arenas *et al.*[34]. For more specific information related to our studies, see Campbell *et al.*[20,21].

Note that assumption (5) posits that each node within the network receives an identical total input from its connected nodes. This is a common approach in neural mass models, particularly when neural tract data is leveraged to construct the connectivity matrix[35–38]. This assumption is often adopted to prevent individual nodes from becoming saturated due to excessive input or quiescent due to insufficient input, thereby facilitating a more equitable comparison of relative strengths between different brain regions[37,38]. As noted above, this assumption also enables the system to exhibit synchronous solutions[39] and is necessary to facilitate direct comparison with the results of Pinder *et al.*[40,41].

C. Numerical methods

We use the `dde23` routine in MATLAB to simulate the system (1) with absolute and relative tolerances set to 10^{-5}. Numerical continuation was performed using DDE-BIFTOOL, a MATLAB package for the numerical bifurcation analysis of DDEs[42].

To compute the maximal Lyapunov exponent, we follow the approach of Sprott[43] and represent the system in (1) by the following infinite-dimensional system of ODEs:

$$\begin{aligned}\dot{\mathbf{x}}_0 &= \mathbf{f}(\mathbf{x}_0, \mathbf{x}_M, \mathbf{x}_N), \\ \dot{\mathbf{x}}_i &= N(\mathbf{x}_{i-1} - \mathbf{x}_i)/\tau,\end{aligned} \tag{6}$$

where $1 \le i \le N \to \infty$ and $\mathbf{f}(\mathbf{x}(t), \mathbf{x}(t-\tau), \mathbf{x}(t-\rho))$ denotes the RHS of the delay-differential system in (1). In the above we have that $\mathbf{x}_M$ and $\mathbf{x}_N$ denote respectively the delayed state variables $\mathbf{x}(t-\tau)$ and $\mathbf{x}(t-\rho)$. Throughout, we assume that the intra-nodal delay, τ, is always smaller than the inter-nodal delay, ρ. We can then compute the maximal Lyapunov exponent by solving the associated variational equations in the usual manner[44]. In all of our experiments, the value of $h = \tau/N = 0.01$ was taken, where h is the grid spacing of our discretisation.

To quantify mean synchrony and metastability within the model, we deploy the Kuramoto order parameter

$$R(t) = \left| \frac{1}{n} \sum_{j=1}^{n} e^{i\theta_j(t)} \right|.$$

Synchrony is then calculated as the mean of R over time, and metastability, S_R, as the standard deviation of R over time. The temporal variability of the order parameter reflects transient fluctuations in neural activity and has previously been employed in both theoretical and empirical investigations to quantify metastability in brain networks[45,46]. Computing the order parameter requires us to extract the instantaneous phase $\theta_j(t)$ of each node, which can be computed by applying the Hilbert transform (implemented in MATLAB using the `hilbert` routine – see[47] for further details) and reading out the angle of the complex output.

D. Network topologies considered

To investigate the impact of network topology on the dynamics of (1) we deploy a range of model network configurations as well a representation of the cortical architecture of the Macaque monkey[25]. More specifically, we consider four toy network structures: a path network, a cycle network, a square lattice and a complete network, all on $N = 16$ nodes. Illustrations of these networks are shown in Figure 1. We chose $N = 16$ since it is large enough to observe network effects but small enough to be computationally efficient (similar results have been observed on larger networks – results not shown). Basic structural properties for each of the toy network models are given in Table I.

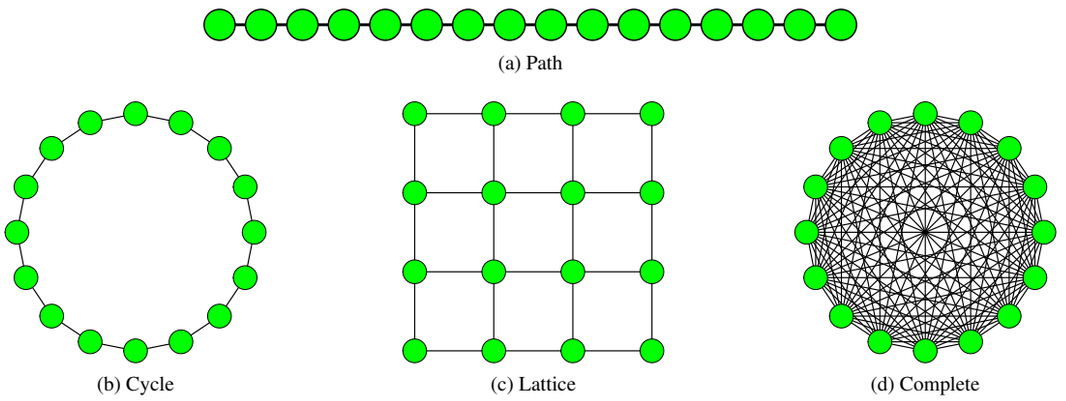

FIG. 1. Illustrations of the toy network models used in our numerical simulations for $N = 16$. We consider (a) path network; (b) cycle network; (c) lattice network; and (d) complete network.

Networks	N	M	$\langle k \rangle$	$\langle l \rangle$	$\langle C \rangle$	σ
Path	16	15	1.875	5.667	0	0.0021
Cycle	16	16	2	4.2667	0	0
Lattice	16	24	3	2.667	0	0.0041
Complete	16	120	15	1	1	0

TABLE I. Structural properties for the toy network architectures considered in this paper.

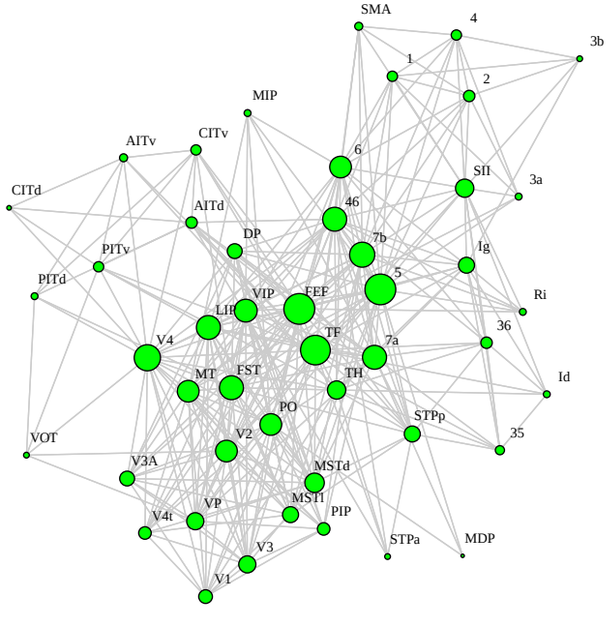

FIG. 2. Structural connectivity network of the Macaque monkey. Node (47 regions of interest) sizes are proportional to degree. Nodes are labelled using standard anatomical abbreviations (see[25] and references therein for further details).

The BNM we consider is composed of Wilson-Cowan nodes coupled according to the adjacency matrix A describing the corticocortical connectivity of the Macaque monkey. Figure 2 displays the Macaque network structure with nodes proportional to the number of connections and labelled according to the standard anatomical atlas. Basic network measures describing this anatomical structure are provided in Table II. It is worth noting that the Macaque network architecture differs markedly from that of the toy networks displayed in Figure 1 in that it simultaneously displays both the small-world property[30] and relatively high levels of heterogeneity[29].

Network	N	M	$\langle k \rangle$	$\langle l \rangle$	$\langle C \rangle$	σ
Macaque	47	313	13.32	1.85	0.64	0.09

TABLE II. Structural properties of the Macaque cortical network.

III. DYNAMICAL REGIMES

In this section, we present a sample of results from the thorough numerical experiments undertaken on the delayed Wilson-Cowan model in (1). We begin by reviewing synchronous solutions of (1), which are seen to be independent of network structure, before proceeding to more complicated network-dependent solutions.

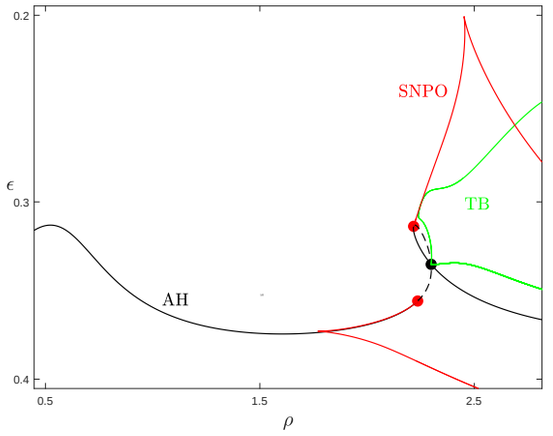

FIG. 3. Two-parameter bifurcation diagram in (ρ,ε) plane for the self-coupled node in (7). The remaining parameter values are as stated in the text. Solid black lines denote supercritical Hopfs and dashed black lines subcritical Hopfs, whilst red circles and black circles denote Bautin and double Hopf bifurcations, respectively. The red curve shows a saddle node of periodic orbits branch emanating from the Bautin bifurcation and the green curve a branch of torus bifurcations emanating from the double Hopf.

A. The synchronous solution and the single, self-coupled node

The model in (1) admits a synchronous solution $(u_i,v_i) = (u_s(t),v_s(t))$, $i = 1,\dots n$, such that the functions $(u_s(t),v_s(t))$ satisfy the single isolated node with delayed self-coupling equation

$$\begin{aligned}\frac{\mathrm{d}u}{\mathrm{d}t} &= -u + f(c_1u(t-\tau)+c_2v(t-\tau)+\varepsilon u(t-\rho)+P)),\\ \frac{\mathrm{d}v}{\mathrm{d}t} &= -v + f(c_3u(t-\tau)+c_4v(t-\tau)+Q),\end{aligned} \tag{7}$$

where we have omitted the subscript s for brevity. It follows that synchronous solutions of (1) can be understood by analysing the behaviour of the simplified model in (7). For example, the point (u^*,v^*) is an equilibrium of (7), independent of the delays ρ and τ, if

$$P = f^{-1}(u^*) - c_1u^* - c_2v^* - \varepsilon u^*, \quad Q = f^{-1}(v^*) - c_3u^* - c_4v^*,$$

where $f^{-1}(z) = \beta^{-1}\ln(z/(1-z))$. We can use direct numerical simulation and numerical continuation techniques to determine solution branches and bifurcations for synchronous solutions of (1).

Figure 3 shows bifurcations for the single, self-coupled node using ε and ρ as parameters of interest. The result is a set of Andronov-Hopf (AH) bifurcations of fixed points in the (ρ,ε) parameter plane corresponding to solutions of (7). Solid black lines correspond to supercritical AH bifurcations and dashed black lines correspond to subcritical AH bifurcations, with changes in criticality separated by Bautin bifurcations, which are labelled with red circles. The AH curve is restricted to $\varepsilon \in [0.3125, 0.3705]$ and possesses a repetitive looping structure (experiments not shown) as ρ is increased; only one such loop is evident from Figure 3. Note that this looping structure results in self-intersections of the AH curve, with each crossing resulting in a double Hopf bifurcation, which we mark by a black circle in Figure 3. The presence of these higher dimensional bifurcations is known to result in increasingly complex dynamics such as mixed mode oscillations and chaos. Saddle node of periodic orbits (SNPO) and torus (TB) bifurcation sets emanating from these higher dimensional bifurcations are displayed by the red and green curves, respectively. It can be shown (experiments omitted) that the system in (7) displays chaotic synchronous dynamics for parameter values within the region bounded by the torus branches, which manifests through the destabilisation of the stable periodic orbit born at the AH branch via a torus bifurcation; this route to chaos is well documented[48]. Outside of this region, the dynamics are either mono- or bi-stable, converging either to a steady state or to a stable periodic orbit, depending upon the choice of the parameters (ρ,ε). For a more detailed description of the bifurcation structure and dynamics of the self-coupled model in (7), we recommend the interested reader consult the recent paper by Pinder *et al.*[41]

Note that the above bifurcation analysis exposes the network's synchronous behaviour, but its relevance depends on whether the network structure inherently disrupts this synchronised state (by inducing instabilities transverse to the synchronous manifold), leading to richer spatiotemporal dynamics. In the remainder of this paper, we aim to broaden our understanding of the system in (1) by examining how network configuration affects the stability of synchronised states under heterogeneous perturbations across diverse network structures.

B. Toy models

To quantify global network dynamics, we measure, for each network, the global level of network synchrony and its variation, *i.e.* metastability, as a function of the network coupling strength, ε, and inter-nodal delay, ρ. The first two columns of Figure 4 depict these two key features of the network dynamics for each of the toy networks considered. As noted earlier, we measure synchronisation as the difference in phase between oscillators, with a score of $\langle R\rangle = 1$ denoting complete synchrony and a score of $\langle R\rangle = 0$ denoting incoherent, desynchronised behaviour. The variation in average synchronisation across the simulation, quantified by $\langle S_R\rangle$, serves as a proxy for metastability. Higher values indicate a more dynamic or transitional regime, where the system fluctuates between periods of synchronised and desynchronised behaviour. To further highlight regions of parameter space in which complex dynamic behaviours exist, the third column in Figure 4 displays, for each toy network, the average maximal Lyapunov exponent (LE) over 100 randomly chosen initial conditions for each choice of (ρ,ε).

The first point to note is that for large couplings, all networks are monostable, with convergence to a stable steady

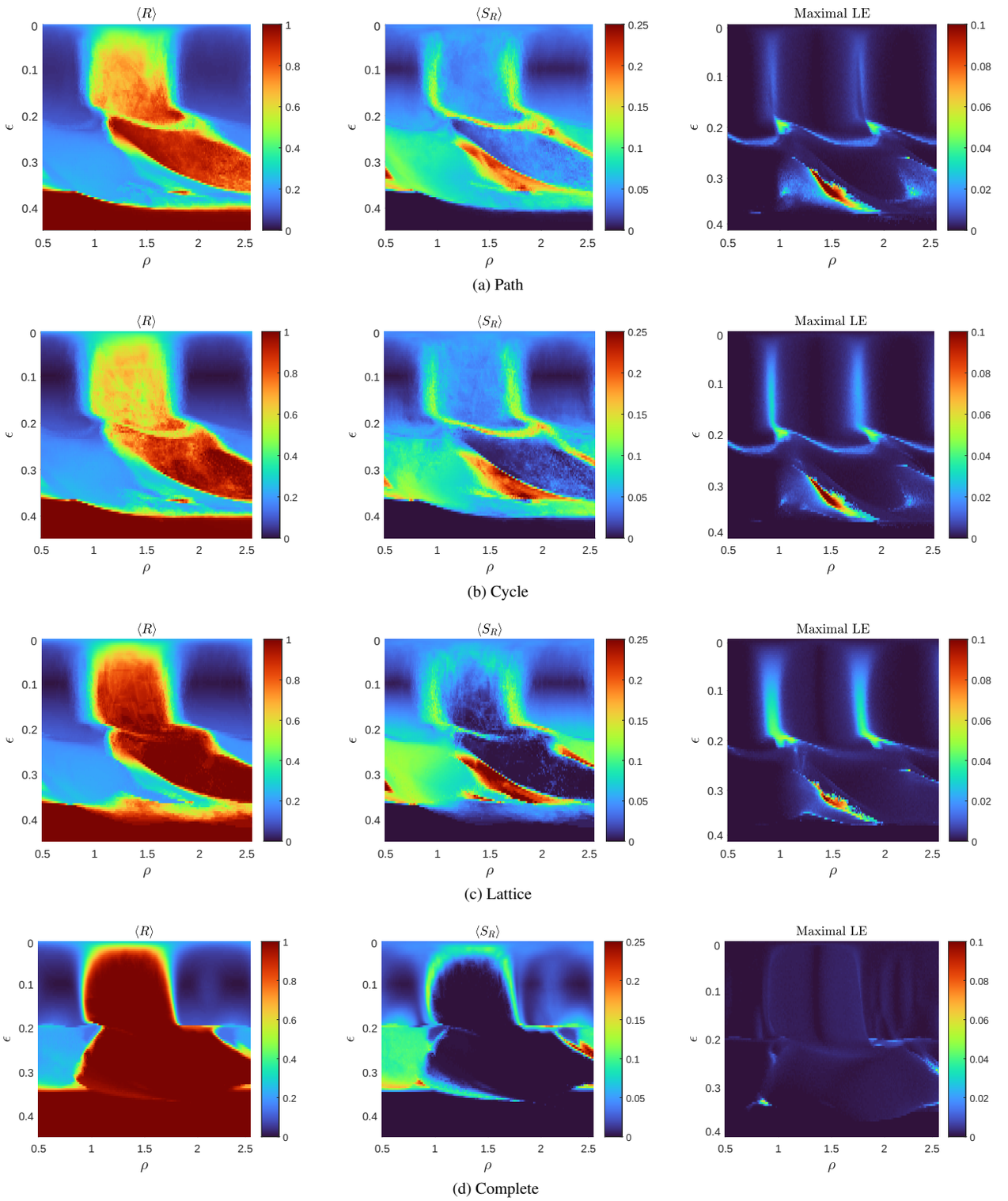

FIG. 4. Global measures of network dynamics for toy network architectures. Left: mean Kuramoto order parameter,$\langle R \rangle$; Middle: mean standard deviation of the Kuramoto order parameter, $\langle S_R \rangle$; and Right: mean largest Lyapanouv exponent. All averages over 100 instances.

state guaranteed independent of the inter-nodal delay ρ. For decreasing values of ε, there are initially two possible (network-independent) behaviours depending upon the value of ρ: either the fixed point loses stability through a Hopf bifurcation; or the system becomes bi-stable after crossing a branch of SNPOs, such as the one displayed in Figure 3, until we reach the first Hopf branch, at which point the steady state destabilises. These regions of stability are clearly delineated in the synchronisation and metastability plots displayed in Figure 4, particularly in the case of the path and cycle networks. In addition to the 'synchronous' Hopf curve shown in Figure 3, for networked systems, we observe additional 'asynchronous' Hopf branches, the number of which increases with network size (experiments not shown; for similar observations in a six-node ring network, see the recent work by Pinder *et al.*[41]). These additional Hopf curves are found to reside within a narrow band of parameter space, with ε lying approximately in the range $[0.3, 0.38]$. Importantly, this leads to an increasing number of branch crossings and higher codimension bifurcations within this region.

For relatively weak coupling strength ($\varepsilon \lesssim 0.2$), all examined network configurations display qualitatively similar dynamics throughout $\rho - \varepsilon$ parameter space, with a central band of high synchronicity and low metastability, as indicated by red and blue areas in the first and second columns of Figure 4, respectively. This regime corresponds to robust, complete synchronisation with very little variability in the case of the lattice and complete networks; whereas the path and cycle networks display moderate levels of synchrony and metastability reflecting fluctuations of the network states as a function of time. Interestingly, in all cases this region of high synchronicity is trapped between two areas of low synchronisation. The boundaries between the highly synchronised region and the low-synchronisation zones are marked by regions of weak chaos (*i.e.*, small, positive LEs), as revealed by the Lyapunov exponent analysis (column three in Figure 4). Our numerical simulations indicate that the synchronous solutions observed in this central region destabilise via a torus bifurcation and that the chaotic boundaries emerge from the breakdown of said torus. This route to chaos is well documented[48].

Intermediate values of coupling strength ($0.2 \lesssim \varepsilon \lesssim 0.4$) lead to increasingly complex, delay-dependent behaviors, as evidenced by regions of intermediate $\langle R \rangle$ and $\langle S_R \rangle$ values and areas of positive maximal LEs. In this region, we observe a heightened sensitivity of the system and a growing coexistence of both stable and unstable periodic orbits as well as more complex aperiodic motions, for all networks except for the complete network. Solutions of the complete network are synchronous for large regions of parameter space, which aligns with Conti and Van Gorder's recent observation[22] that well-connected, uniform networks display high synchrony levels regardless of delay or coupling strength. Within our chosen parameter range, the complete network fails to generate complex spatiotemporal patterns. Instead, non-synchronised activity manifests as either antiphase or out-of-phase oscillations. Note that the observed increase in network dynamics complexity (see Figure 4) is a natural consequence of the aforementioned Hopf branch crossings. These crossings are known to trigger a cascade of higher-order bifurcations, such as the double Hopf and Bautin bifurcations observed in Figure 3. Furthermore, the presence of these codimension-two bifurcations generically leads to the emergence of additional branches, which leads to complicated basin boundary structures and increasingly multistable behaviours.

C. Macaque cortical network topology

In this section, we simulate functionally realistic dynamics by deploying the known large-scale cortical architecture of the Macaque monkey alongside the neural mass model in (1) to model the dynamics in each node (or brain region). Our results are shown in figures 5, 6 and 7.

Building on our previous experiments, Figure 5 displays the results for the cortical network. We plot the mean synchrony and metastability scores and the maximum Lyapunov exponent as functions of the parameters ε and ρ. These values represent the averages obtained over 100 independent simulations, each initialised with a different random configuration. In addition, we have superimposed the lower envelope of the Hopf bifurcation branches (both synchronous and asynchronous), which separates the parameter space in to regions were the system either converges to a stable equilibrium or limit cycle (multi-stability can arise via a SNPO bifurcation as in Figure 3) from regions characterised by unstable equilibria, limit cycles and more complicated behaviours. Notably, the findings for the cortical network exhibit a striking resemblance to those observed for the complete network (Figure 4(d)), but with two major differences. First, for the cortical network we identify regions of parameter space (as shown in the maximal LE plot of Figure 5(c)) that allow for chaotic dynamics. Second, we observe an island of heightened metastability located just above the Hopf envelope and towards the center of the picture.

Exemplar solutions for three different choices of parameter values (ρ, ε) as well as a snapshot of the instantaneous phases are displayed in Figure 6. In Figure 5(a), we highlight by a circle, square and triangle, the parameter values corresponding to the simulated solutions shown in figures 6(a), 6(b), and 6(c), respectively. The first two panels in Figure 6 depict contrasting out-of-phase behaviors: panel (a) shows an approximate antiphase solution, while panel (b) displays an incoherent out-of-phase solution. Panel (c) depicts a solution generated using parameters selected from the aforementioned high-metastability region. Crucially, the solutions with these parameter values exhibit time-dependent behaviors unique to the cortical network. In contrast to other configurations, for these parameter values we observe oscillations in which phases are tightly clustered but amplitudes remain desynchronised (as shown in Figure 6(c), left panel). More specifically, the network nodes appear to form phase-cluster states (or cluster synchronisation[49]) whereby groups of nodes exhibit different yet approximate synchronised phase dynamics within each group (Figure 6(c), right panel).

To investigate the observed phase clustering, which is in-

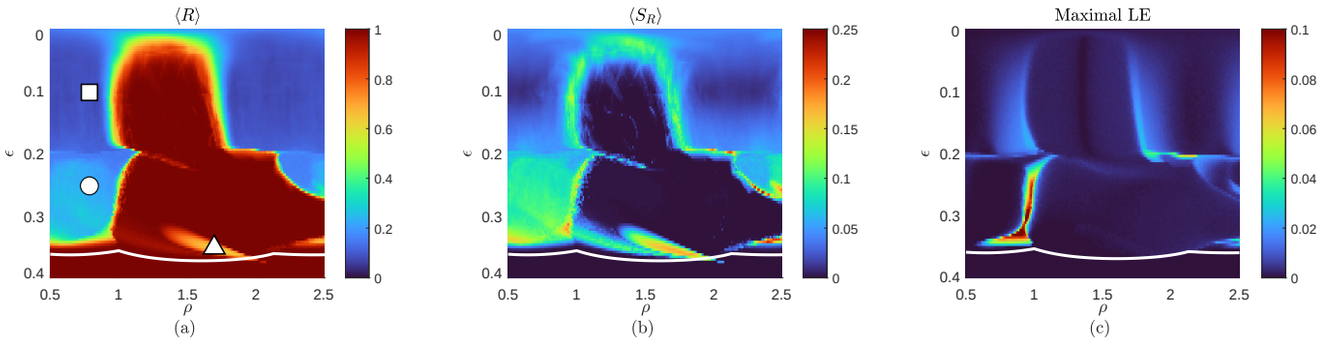

FIG. 5. Global measures of network dynamics for the Macaque connectome. (a) mean Kuramoto order parameter, $\langle R \rangle$; (b) mean standard deviation of the Kuramoto order parameter, $\langle S_R \rangle$; and (c) mean largest Lyapanouv exponent. All averages over 100 instances.

dicative of the modular brain connectivity structures typically observed in contemporary imaging studies[50], we constructed a model of functional connectivity (FC) using mean phase coherence. This method quantifies synchrony levels between the simulated activity of each cortical region and is defined as the temporal mean of the difference in instantaneous phases between each brain region (see the paper by Mormann *et al.*[47] for further details). Figure 7(a) shows a space-time plot for the excitatory variable $u_i(t)$ with network nodes ordered from lowest to highest value of u_i at a fixed time, which results in temporally coherent wave-like patterns that exhibit negligible spatial spread. While Figure 7(b) provides a visual representation of the FC matrix derived from the time series data presented in Figure 7(a). To focus on stable network behaviors, the initial period of the simulation ($t < 100$) was excluded from the analysis of the FC matrix. This ensures the FC reflects a long-term, consistent pattern rather than capturing temporary fluctuations present at the beginning of the simulation.

From Figure 7(b) we observe clusters of highly correlated nodes in the brain network. Importantly, this type of segregation was not evidenced in any of our simulations for the mathematically constructed networks, suggesting that the heterogeneity manifest within the real-world cortical connectivity structure is crucial for creating the dynamic conditions that allow for these partially synchronised patterns to emerge. Moreover, for this choice of parameter values we find that the network is capable of attaining a range of functional configurations upon variation of the initial conditions. Some indicative examples are shown in Figure 8. The identified region appears to promote a set of dense highly variable functional states, organised across multiple hierarchical levels, that are readily accessible, thereby supporting the brain's necessary ability to switch easily between a variety of states. This is a manifestation of the heightened levels of metastability in this region of parameter space and provides evidence of the necessary interplay between network structure and time delay that supports the brain's flexible and dynamic repertoire of higher brain function.

D. Chaotic nodes

For the Macaque network we also considered the case in which individual nodes (*i.e.* uncoupled with $\varepsilon = 0$) displayed chaotic behaviour. In order to do this, we changed the following parameters:

$$c_1 = c_4 = -6,\ c_2 = c_3 = 2.5,\ P = Q = 0.2 \quad \text{and} \quad \tau = 0.1.$$

This choice of parameters has been shown to induce chaotic behaviour in a single delayed Wilson-Cowan node[33]. All other parameters remain unchanged.

It has previously been reported in the case of toy network models that delays can induce a regularising effect in the dynamics[22], and it is of interest to consider whether these results are replicated in the case of a cortical network. Figure 9(a,b,c) shows respectively the mean order parameter, metastability and maximal LE for the Macaque network with parameters chosen so that the uncoupled system displays chaotic behaviour. The first point of note is that stronger coupling is required to trigger significant self-organised synchronisation in a cortical network comprised of chaotic nodes. However, for sufficiently strong coupling we observe large regions of robust synchronisation, *i.e.*, areas of parameter space in which $\langle R \rangle$ is high and $\langle S_R \rangle$ is low, as well as intermittent regions of parameter space that present moderate levels of synchrony and fluctuations, as measured by $\langle R \rangle$ and $\langle S_R \rangle$ – see figures 9(a, b). Moreover, as evidenced by Figure 9(c), the resultant sychronised signals are generally chaotic, with parameter space dominated by extensive regions of positive LEs. Nevertheless, for very strong levels of coupling strengths ($\varepsilon \geq 3$), variations in the inter-nodal delay (ρ) give rise to intermittent periods of weak chaotic behavior and coherent oscillatory patterns. Furthermore, a localised region of stability emerges at the center of the parameter plane, as most clearly illustrated in the LE plot (Figure 9(c)). Solutions from this region are defined by the presence of a stable limit cycle that emerges for the cortical topology under variation of the parameters (ρ, ε).

Exemplar solutions for three different choices of parameter values (ρ, ε) as well as a snapshot of the instantaneous phases are displayed in Figure 10. In Figure 9(c), we highlight by a

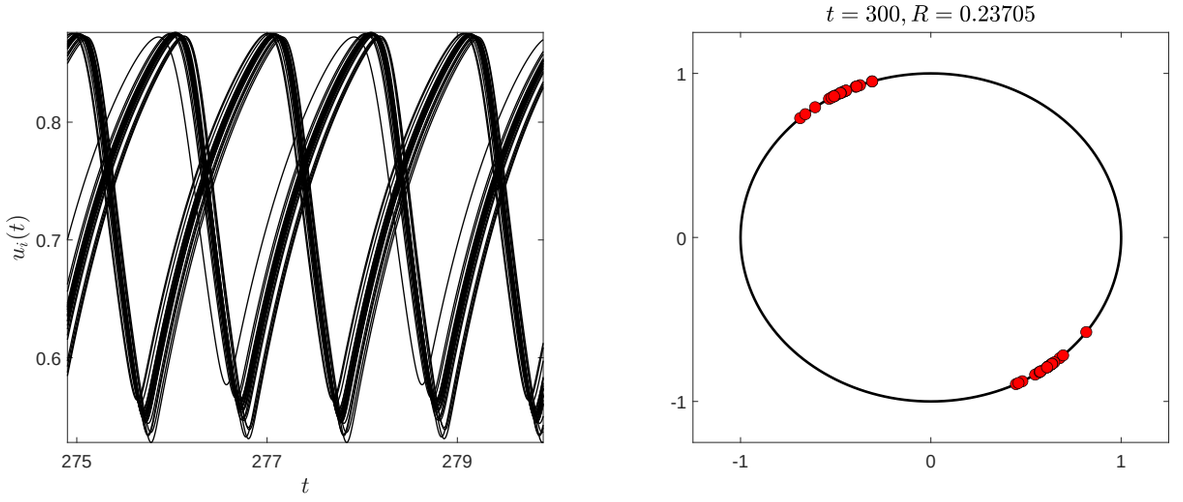

(a) $(\rho, \varepsilon) = (0.75, 0.25)$

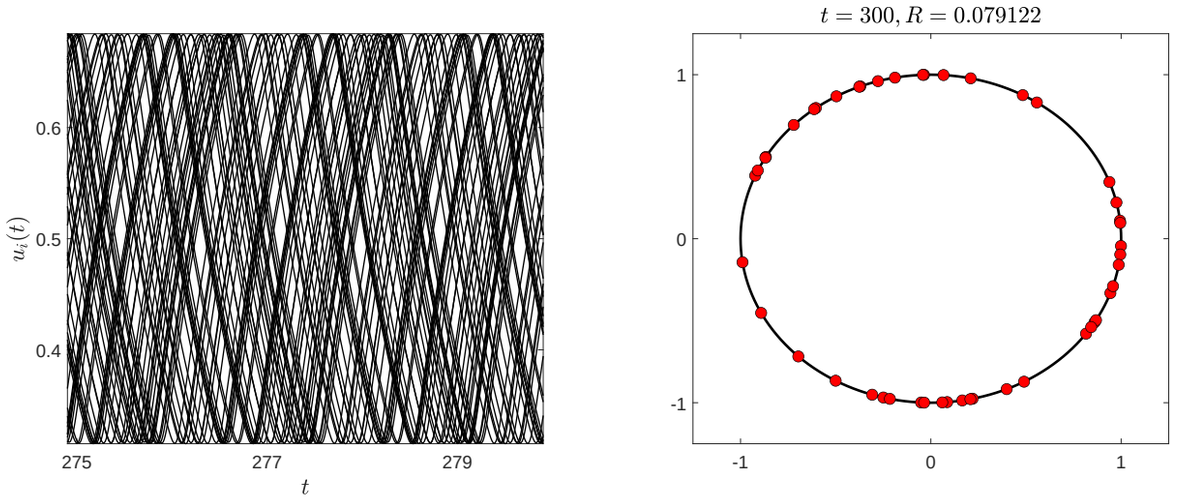

(b) $(\rho, \varepsilon) = (0.75, 0.10)$

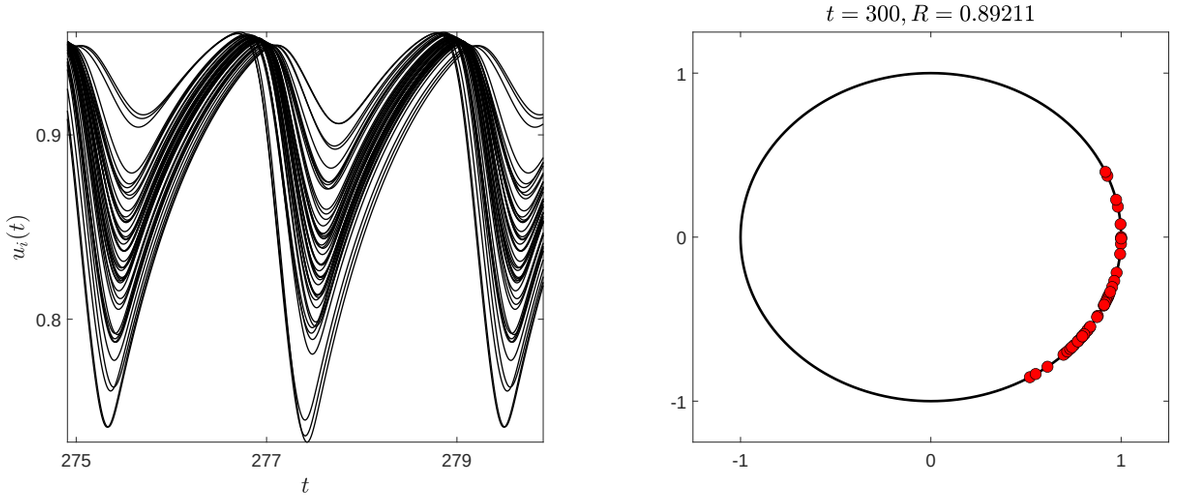

(c) $(\rho, \varepsilon) = (1.75, 0.37)$

FIG. 6. Left: exemplar solutions of (1) for three different choices of parameter values (ρ, ε) and connectivity structure given by the Macaque connectome. Right: for each of the solutions, we plot a snapshot of the instantaneous phase on the unit circle.

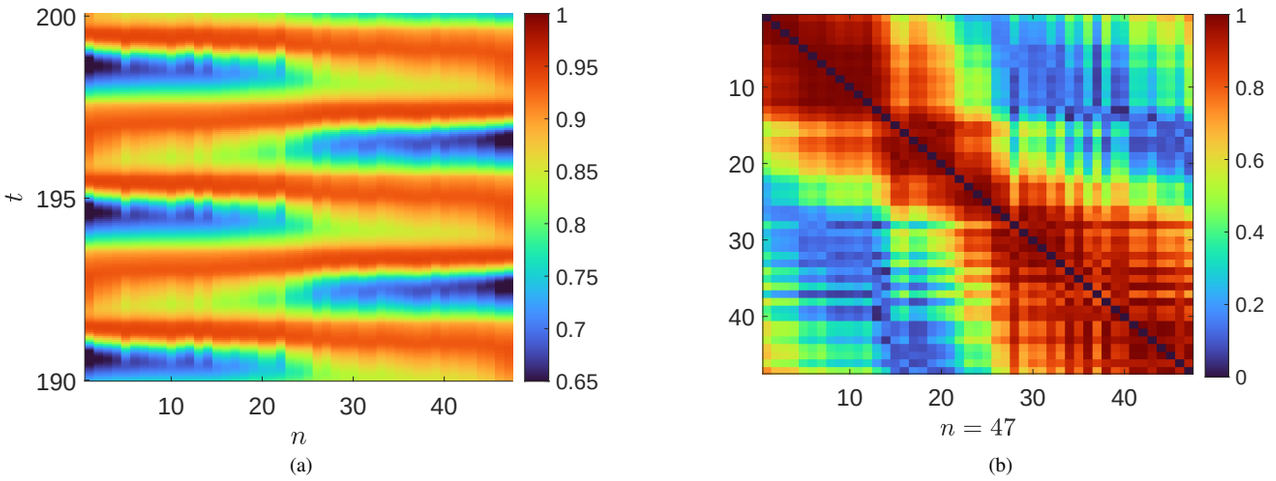

FIG. 7. (a) Space-time plot of the excitatory variable u_i with $(\rho, \varepsilon) = (1.75, 0.37)$. Oscillators are reordered from the lowest to the highest value of u_i at a fixed time. (b) Functional connectivity network obtained by computing the mean phase coherence of the time series displayed in (a).

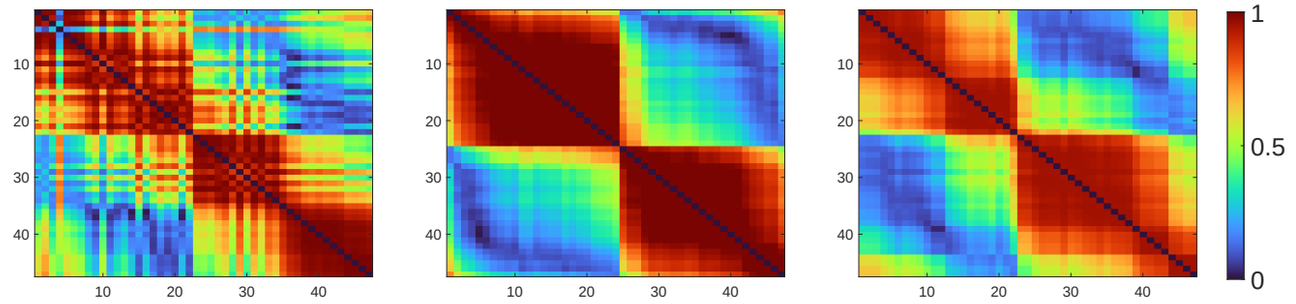

FIG. 8. Simulated functional connectivity matrices with specific parameter values $(\rho, \varepsilon) = (1.75, 0.37)$, which are highlighted by a triangle in Figure 5. For these parameter values the network is capable of attaining a range of functional configurations, (a)-(c), under variation of the initial conditions.

square, circle and triangle, the parameter values corresponding to to the simulated solutions shown in figures 10(a), 10(b) and 10(c), respectively. The first two panels in Figure 10 depict two contrasting chaotic behaviours: panel (a) illustrates an unsynchronised chaotic solution, while panel (b) showcases an approximately synchronised chaotic solution. Panel (c) depicts a solution in which the network dynamics have synchronised and dynamic regularity has been recovered.

These results suggest that cortical structure can regulate aperiodic network behavior via a balanced interplay between coupling strength and delays, thus extending the results of Conti and Van Gorder[22] to empirical brain networks. This observation is of relevance to the neuroimaging application that is our focus here, since it suggests that network delays may play a key role in preventing the appearance and spread of pathological dynamics, such as those observed in seizure disorders.

IV. DISCUSSION

The intricate network architecture observed in the brain (complex network topology) poses a challenge to understanding its function. To address this, we compared the dynamic behavior of a network based on real, structural neural connections obtained from tracer studies with various theoretical network models. Our brain network model, based on the delayed Wilson-Cowan framework for individual node activity, revealed a surprisingly consistent pattern of dynamic behavior across all network structures investigated. These regimes encompassed fully synchronised states, partially synchronised states with fluctuating coherence, and even irregular activity reminiscent of chaos. At low coupling strengths, the parameter space exhibits a repetitive striping pattern, independent of the network structure. These alternating stripes indicate regions where brain activity is either synchronised (equal phases and amplitudes) or non-synchronised (out of phase).

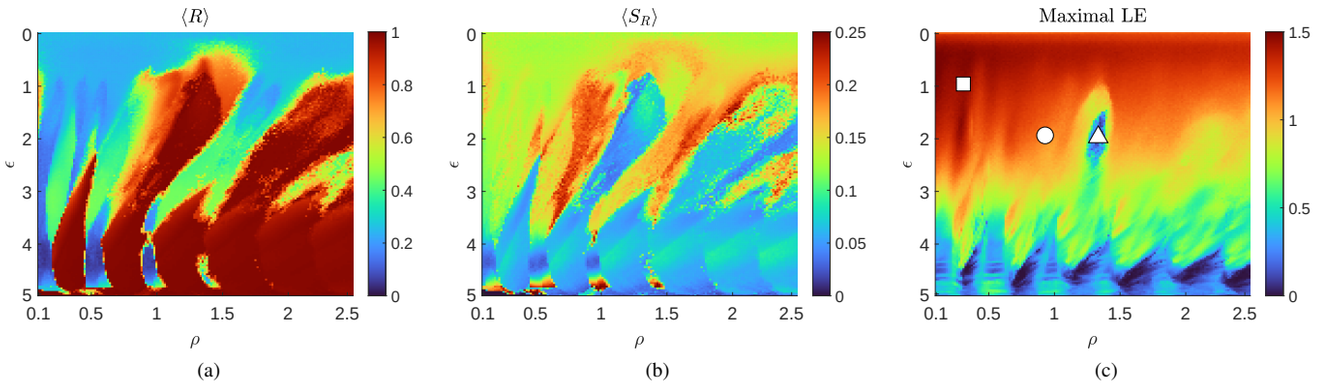

FIG. 9. Global measures of network dynamics for the Macaque connectome with parameters chosen so that the uncoupled system displays chaotic behaviour. (a) mean Kuramoto order parameter,$\langle R\rangle$; (b) mean standard deviation of the Kuramoto order parameter, $\langle S_R\rangle$; and (c) mean largest Lyapanouv exponent. All averages over 100 instances.

The interfaces between these striped regimes are delineated by regions exhibiting weak chaos (see figures 4 and 5). Numerical simulations suggest that this weak chaos originates from transverse instabilities within the synchronisation manifold due to a torus breakdown. For similar results on a 6-node ring network, see the recent paper by Pinder *et al.*[41]. Increasing the coupling strength reveals a progressively intricate dynamical landscape. This arises from intersections of Hopf branches alongside branches originating from higher-order bifurcations associated with the Hopf bifurcations themselves. Consequently, this regime exhibits intricate multistable dynamics across all network configurations except the complete network, which exhibits a high propensity for synchronisation.

As well as the cortical network of the Macaque monkey, we considered four toy network structures, namely path, cycle, lattice and complete networks. We observed that sparsely connected networks with low clustering coefficients (path, cycle, and lattice) exhibit reduced synchronisation capabilities compared to densely connected networks (complete network and cortical network). These results corroborate the findings of Conti and Van Gorder[22], who demonstrated the instability of sparsely connected networks, as well as numerous previous studies on both model and empirical networks (see Arenas *et al.*[34]). We found the complete network, with its increased density of connections, served as the closest model for the synchrony observed in the cortical network; the brain's structure, however, goes beyond simple synchrony. It additionally supports novel wave forms and other intricate patterns not observed in the toy networks. For the cortical network, we identified an operational region conducive to flexible brain operations. This region harbours a dense, hierarchically organised set of distinct functional states that are readily accessible, facilitating the type of state-switching essential for higher cognitive function. The observed modular FC patterns closely resemble those found in imaging studies and, crucially, were not replicated in any of the toy network simulations. These segregated FC patterns likely arise from the inherent modular heterogeneity of the brain's structural connectivity, as described by Sporns *et al.*[51].Notably, the brain also exhibits incoherent, chaotic-like dynamics, a property absent in the complete network. In fact, the complete network is the only structure lacking this behaviour. This can be attributed to the inherent homogeneity of its degree distribution, where all nodes possess identical connection numbers.

To isolate the impact of inter-nodal delays, we initially focused on networks with local dynamics exhibiting a single-frequency oscillation. However, we also investigated how these findings translate to a more realistic cortical network with chaotic local dynamics, thus extending the work of Conti and Van Gorder[22] to a more physiologically realistic setting. While chaotic behavior (both synchronised and unsynchronised) dominated our observations, we found that careful calibration of coupling strength and inter-nodal delay could still promote regularised neural network dynamics. This result is particularly interesting from a neuroscience perspective, since, despite its chaotic nature, our brain network model was still capable of achieving 'coordinated function', which is suggests that delays can play a role in preventing the appearance of pathological spreading behaviour.

Future research will investigate how to integrate additional physiological details into the model. This includes accounting for the heterogeneity of signal transmission velocities across connections based on factors like distance, myelination levels, and axon thickness. It would also be interesting to see how our results are altered under a signal transmission model that represents more accurately the behaviour of a neural unit, such as the Jansen-Ritt[8] or next-generation models[10,52–54], which are better equipped to capture the intricacies of neuronal synchronisation. Moreover, given the relatively low heterogeneity of the toy networks studied here, it would be valuable to extend this research to compare synchrony dynamics in brain network models with those of more complex network models, such as the Watts-Strogatz small-world model and random network models that preserve degree structure. Finally, a small number of recent studies have emphasised the importance of properly accounting for network directionality[55–57], and so it would be of great interest to investigate the impact of

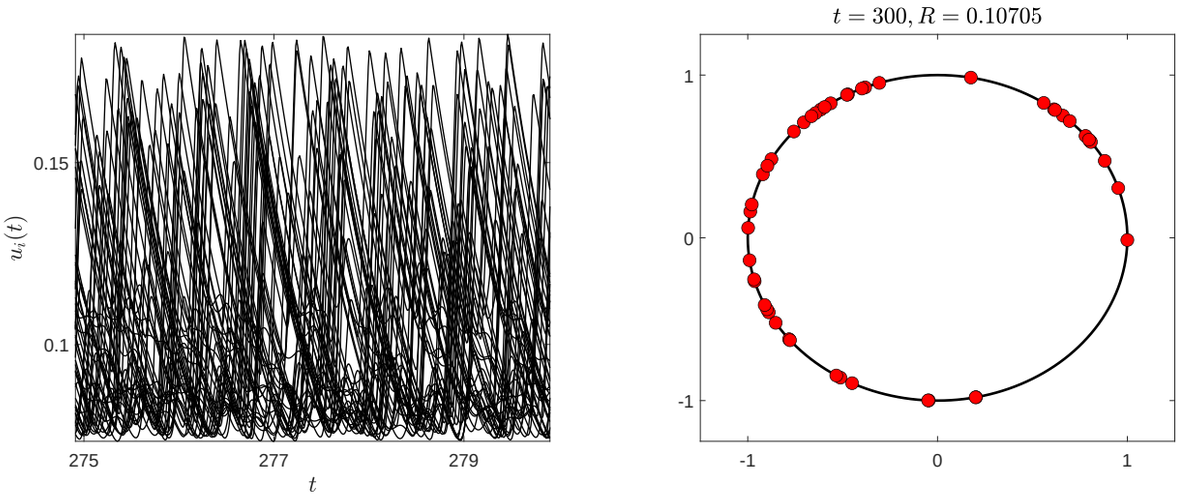

(a) $(\rho, \varepsilon) = (0.30, 0.95)$

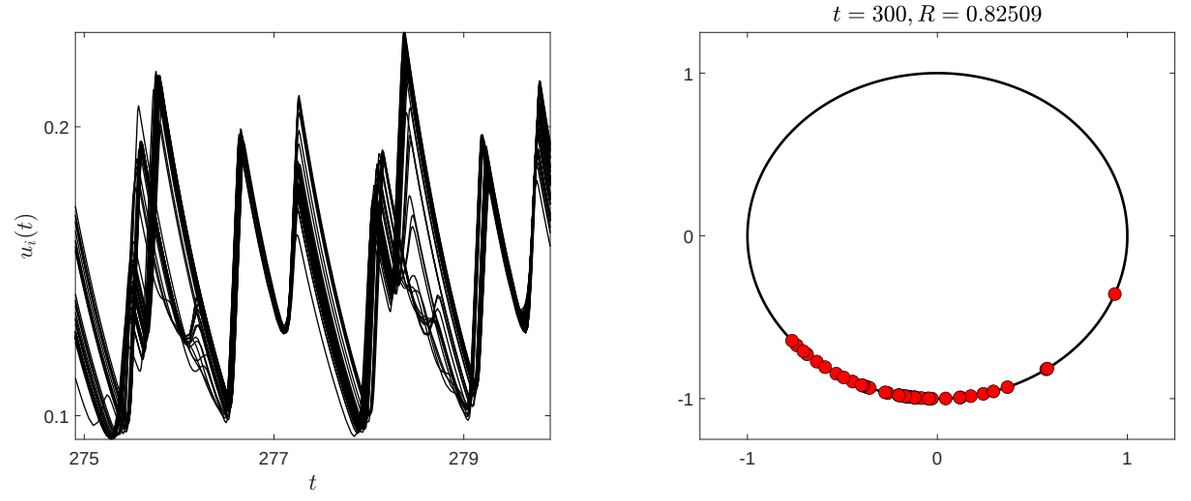

(b) $(\rho, \varepsilon) = (0.90, 1.95)$

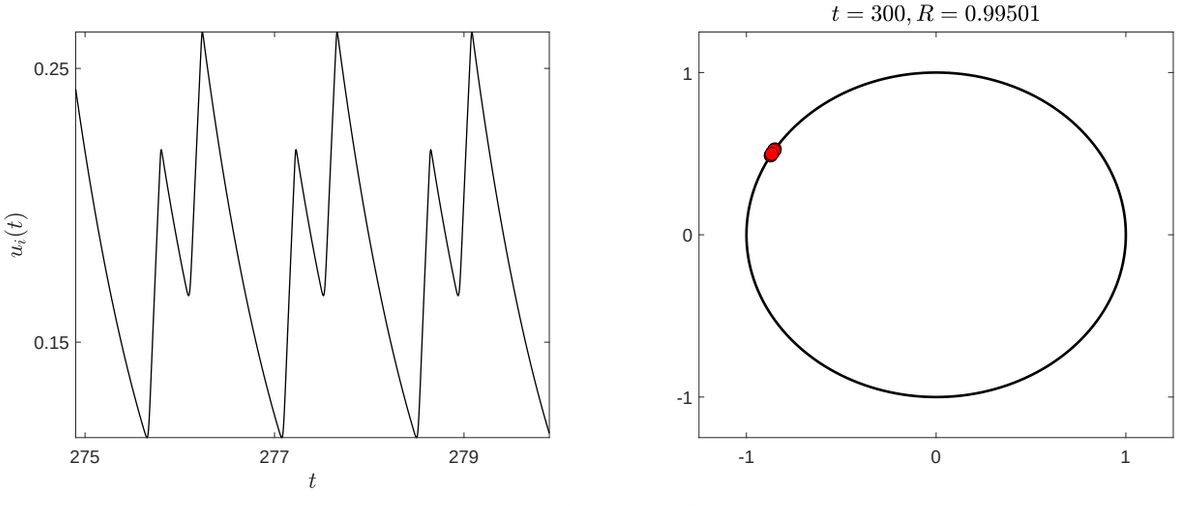

(c) $(\rho, \varepsilon) = (1.35, 2.00)$

FIG. 10. Network dynamics for the Macaque connectome with parameters chosen so that the uncoupled system displays chaotic behaviour. Left: exemplar solutions under variation of the inter-nodal delay, ρ, and coupling strength, ε. Right: for each of the solutions, we plot a snapshot of the instantaneous phase on the unit circle.

network directionality on the results presented in this work.

[1]O. Sporns, *Networks of the Brain* (MIT Press, 2010).
[2]S. Coombes, "Large-scale neural dynamics: simple and complex," NeuroImage **52**, 731–739 (2010).
[3]M. Kaiser, "A tutorial in connectome analysis: topological and spatial features of brain networks," NeuroImage **57**, 892–907 (2011).
[4]G. Buzsaki and A. Draguhn, "Neuronal oscillations in cortical networks," Science **304**, 1926–1929 (2004).
[5]M. Rubinov, O. Sporns, C. van Leeuwen, and M. Breakspear, "Symbiotic relationship between brain structure and dynamics," BMC Neuroscience **10**, 55 (2009).
[6]G. Deco, A. Ponce-Alvarez, D. Mantini, G. L. Romani, P. Hagmann, and M. Corbetta, "Resting-state functional connectivity emerges from structurally and dynamically shaped slow linear fluctuations," Journal of Neuroscience **33**, 11239–11252 (2013).
[7]M. Breakspear, "Dynamic models of large-scale brain activity," Nature Neuroscience **20**, 340 (2017).
[8]M. Forrester, S. Coombes, J. J. Crofts, S. N. Sotiropoulos, and R. O'Dea, "The role of node dynamics in shaping emergent spatial functional connectivity patterns in the brain," Network Neuroscience **4**, 467–483 (2020).
[9]P. Sanz-Leon, S. A. Knock, A. Spiegler, and V. K. Jirsa, "Mathematical framework for large-scale brain network modeling in the virtual brain," NeuroImage **111**, 385–430 (2015).
[10]Á. Byrne, R. D. O'Dea, M. Forrester, J. Ross, and S. Coombes, "Next-generation neural mass and field modeling," Journal of Neurophysiology **123**, 726–742 (2020).
[11]M. Gerster, H. Taher, A. Škoch, J. Hlinka, M. Guye, F. Bartolomei, V. Jirsa, A. Zakharova, and S. Olmi, "Patient-specific network connectivity combined with a next generation neural mass model to test clinical hypothesis of seizure propagation," Frontiers in Systems Neuroscience **15**, 675272 (2021).
[12]M. Sacha, J. S. Goldman, L. Kusch, and A. Destexhe, "Asynchronous and slow-wave oscillatory states in connectome-based models of mouse, monkey and human cerebral cortex," Applied Sciences **14**, 1063 (2024).
[13]V. Jirsa, O. Sporns, M. Breakspear, G. Deco, and A. R. McIntosh, "Towards the virtual brain: network modeling of the intact and the damaged brain," Archives Italiennes de Biologie **148**, 189–205 (2010).
[14]J. Vohryzek, J. Cabral, F. Castaldo, Y. Sanz-Perl, L.-D. Lord, H. Fernandes, V. Litvak, M. L. Kringelbach, and G. Deco, "Dynamic sensitivity analysis: Defining personalised strategies to drive brain state transitions via whole brain modelling," Computational and Structural Biotechnology Journal (2022).
[15]V. Jirsa, H. Wang, P. Triebkorn, M. Hashemi, J. Jha, J. Gonzalez-Martinez, M. Guye, J. Makhalova, and F. Bartolomei, "Personalised virtual brain models in epilepsy," The Lancet Neurology **22**, 443–454 (2023).
[16]S. A. Campbell, "Time delays in neural systems," Handbook of Brain Connectivity , 65–90 (2007).
[17]G. Deco, V. Jirsa, A. R. McIntosh, O. Sporns, and R. Kötter, "Key role of coupling, delay, and noise in resting brain fluctuations," Proceedings of the National Academy of Sciences **106**, 10302–10307 (2009).
[18]S. Petkoski and V. K. Jirsa, "Transmission time delays organize the brain network synchronization," Philosophical Transactions of the Royal Society A **377**, 20180132 (2019).
[19]G. Rabuffo, J. Fousek, C. Bernard, and V. Jirsa, "Neuronal cascades shape whole-brain functional dynamics at rest," Eneuro **8** (2021).
[20]W. Nicola, P. J. Hellyer, S. A. Campbell, and C. Clopath, "Chaos in homeostatically regulated neural systems," Chaos: An Interdisciplinary Journal of Nonlinear Science **28**, 083104 (2018).
[21]I. Al-Darabsah, L. Chen, W. Nicola, and S. A. Campbell, "The impact of small time delays on the onset of oscillations and synchrony in brain networks," Frontiers in Systems Neuroscience **15**, 688517 (2021).
[22]F. Conti and R. A. Van Gorder, "The role of network structure and time delay in a metapopulation wilson–cowan model," Journal of Theoretical Biology **477**, 1–13 (2019).
[23]H. R. Wilson and J. D. Cowan, "Excitatory and inhibitory interactions in localized populations of model neurons," Biophysical Journal **12**, 1 – 24 (1972).
[24]K. E. Stephan, L. Kamper, A. Bozkurt, G. A. Burns, M. P. Young, and R. Kötter, "Advanced database methodology for the collation of connectivity data on the macaque brain (cocomac)," Philosophical Transactions of the Royal Society of London. Series B: Biological Sciences **356**, 1159–1186 (2001).
[25]R. Bakker, T. Wachtler, and M. Diesmann, "Cocomac 2.0 and the future of tract-tracing databases," Frontiers in Neuroinformatics **6**, 30 (2012).
[26]E. Tognoli and J. S. Kelso, "The metastable brain," Neuron **81**, 35–48 (2014).
[27]T. Nishikawa, A. E. Motter, Y.-C. Lai, and F. C. Hoppensteadt, "Heterogeneity in oscillator networks: Are smaller worlds easier to synchronize?" Physical Review Letters **91**, 014101 (2003).
[28]A. E. Motter, C. Zhou, and J. Kurths, "Network synchronization, diffusion, and the paradox of heterogeneity," Physical Review E **71**, 016116 (2005).
[29]E. Estrada, "Quantifying network heterogeneity," Physical Review E **82**, 066102 (2010).
[30]D. J. Watts and S. H. Strogatz, "Collective dynamics of 'small-world'networks," Nature **393**, 440–442 (1998).
[31]D. S. Bassett and E. T. Bullmore, "Small-world brain networks revisited," The Neuroscientist **23**, 499–516 (2017).
[32]M. Newman, *Networks* (Oxford University Press, 2018).
[33]S. Coombes and C. Laing, "Delays in activity-based neural networks," Philosophical Transactions of the Royal Society A: Mathematical, Physical and Engineering Sciences **367**, 1117–1129 (2009).
[34]A. Arenas, A. Díaz-Guilera, J. Kurths, Y. Moreno, and C. Zhou, "Synchronization in complex networks," Physics Reports **469**, 93–153 (2008).
[35]J. Hlinka and S. Coombes, "Using computational models to relate structural and functional brain connectivity," European Journal of Neuroscience **36**, 2137–2145 (2012).
[36]J. J. Crofts, M. Forrester, and R. D. O'Dea, "Structure-function clustering in multiplex brain networks," Europhysics Letters **116**, 18003 (2016).
[37]T. Kunze, A. Hunold, J. Haueisen, V. Jirsa, and A. Spiegler, "Transcranial direct current stimulation changes resting state functional connectivity: A large-scale brain network modeling study," NeuroImage **140**, 174–187 (2016).
[38]W. Nicola and S. A. Campbell, "Normalized connectomes show increased synchronizability with age through their second largest eigenvalue," SIAM Journal on Applied Dynamical Systems **20**, 1158–1176 (2021).
[39]P. Clusella, G. Deco, M. L. Kringelbach, G. Ruffini, and J. Garcia-Ojalvo, "Complex spatiotemporal oscillations emerge from transverse instabilities in large-scale brain networks," PLOS Computational Biology **19**, e1010781 (2023).
[40]I. Pinder and J. J. Crofts, "Oscillations and synchrony in a network of delayed neural masses," in *Rhythmic Oscillations in Proteins to Human Cognition* (Springer, 2021) pp. 187–211.
[41]I. Pinder, M. Nelson, and J. Crofts, "Bifurcations and synchrony in a ring of delayed Wilson–Cowan oscillators," Proceedings of the Royal Society A **479**, 20230313 (2023).
[42]K. Engelborghs, T. Luzyanina, and D. Roose, "Numerical bifurcation analysis of delay differential equations using dde-biftool," ACM Transactions on Mathematical Software (TOMS) **28**, 1–21 (2002).
[43]J. Sprott, "A simple chaotic delay differential equation," Physics Letters A **366**, 397–402 (2007).
[44]J. C. Sprott, *Chaos and time-series analysis*, Vol. 69 (Oxford University Press, 2003).
[45]V. Vuksanović and P. Hövel, "Dynamic changes in network synchrony reveal resting-state functional networks," Chaos: An Interdisciplinary Journal of Nonlinear Science **25** (2015).
[46]M. Mackay, S. Huo, and M. Kaiser, "Spatial organisation of the mesoscale connectome: A feature influencing synchrony and metastability of network dynamics," PLoS Computational Biology **19**, e1011349 (2023).
[47]F. Mormann, K. Lehnertz, P. David, and C. E. Elger, "Mean phase coherence as a measure for phase synchronization and its application to the eeg of epilepsy patients," Physica D: Nonlinear Phenomena **144**, 358–369 (2000).
[48]H. Ju, A. B. Neiman, and A. L. Shilnikov, "Bottom-up approach to torus bifurcation in neuron models," Chaos: An Interdisciplinary Journal of Nonlinear Science **28**, 106317 (2018).
[49]M. Lodi, S. Panahi, F. Sorrentino, A. Torcini, and M. Storace, "Patterns of synchronized clusters in adaptive networks," Communications Physics **7**, 198 (2024).
[50]D. Meunier, R. Lambiotte, and E. T. Bullmore, "Modular and hierarchically modular organization of brain networks," Frontiers in Neuroscience **4**, 7572

(2010).
[51]O. Sporns and R. F. Betzel, "Modular brain networks," Annual Review of Psychology **67**, 613–640 (2016).
[52]E. Montbrió, D. Pazó, and A. Roxin, "Macroscopic description for networks of spiking neurons," Physical Review X **5**, 021028 (2015).
[53]S. Coombes and Á. Byrne, "Next generation neural mass models," in *Nonlinear Dynamics in Computational Neuroscience*, edited by F. Corinto and A. Torcini (Springer International Publishing, Cham, 2019) pp. 1–16.
[54]S. Coombes, "Next generation neural population models," Frontiers in Applied Mathematics and Statistics **9**, 1128224 (2023).
[55]M. Asllani, J. D. Challenger, F. S. Pavone, L. Sacconi, and D. Fanelli, "The theory of pattern formation on directed networks," Nature Communications **5**, 4517 (2014).
[56]A. Padmore, M. R. Nelson, N. Chuzhanova, and J. J. Crofts, "Modelling the impact of structural directionality on connectome-based models of neural activity," Journal of Complex Networks **8**, cnaa033 (2020).
[57]J. Crofts, N. Chuzhanova, A. Padmore, and M. Nelson, "Synchrony in directed connectomes," Europhysics Letters **139**, 42004 (2022).